Analytica Chimica Acta 814 (2014) 31–38

Contents lists available at ScienceDirect

Analytica Chimica Acta

journal homepage: www.elsevier.com/locate/aca

Electrochemical biosensor based on self-assembled monolayers modified with gold nanoparticles for detection of HER-3

Mehmet Çetin Canbaz, Çiğdem Sayıklı Şimşek, Mustafa Kemal Sezgintürk*

Namık Kemal University, Faculty of Science and Arts, Chemistry Department, Biochemistry Division, Tekirdağ, Turkey

HIGHLIGHTS

- Single frequency impedance technique was firstly used for characterization of interaction between HER-3 and anti-HER-3.
- Anti-HER-3 antibody was firstly utilized in an immunosensor as a bioreceptor.
- The biosensor exhibits high analytical performance with a linear range 0.2–1.4 pg mL^{-1}.
- Kramers–Kronig transform was successfully performed on the experimental impedance data.

GRAPHICAL ABSTRACT

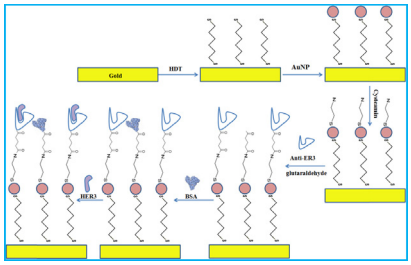

ARTICLE INFO

Article history:
Received 2 August 2013
Received in revised form
18 December 2013
Accepted 16 January 2014
Available online 23 January 2014

Keywords:
Cancer biomarkers
HER-3
Anti-HER-3
Single frequency impedance
Biosensor

ABSTRACT

We have developed a new immunological biosensor for ultrasensitive quantification of human epidermal growth factor receptor-3(HER-3). In order to construct the biosensor, the gold electrode surface was layered with, hexanedithiol, gold nanoparticles, and cysteamine, respectively. Anti-HER-3 antibody was covalently attached to cysteamine by glutaraldehyde and used as a bioreceptor in a biosensor system for the first time by this study. Surface characterization was obtained by means of electrochemical impedance spectroscopy and voltammetry. The proposed biosensor showed a good analytical performance for the detection of HER-3 ranging from 0.2 to 1.4 pg mL^{-1}. Kramers–Kronig transform was performed on the experimental impedance data. Moreover, in an immunosensor system, the single frequency impedance technique was firstly used for characterization of interaction between HER-3 and anti-HER-3. Finally the presented biosensor was applied to artificial serum samples spiked with HER-3.

1. Introduction

The human epidermal growth factor receptor (HER) family plays a key role in regulation of mammalian cell survival, proliferation, adhesion, and differentiation. This HER family of receptor tyrosine kinases comprises four structurally related transmembrane receptors: HER-1 (EGFR or c-erbB-1), HER-2 (HER-2neu or c-erb-B-2), HER-3 (c-erb-B-3), and HER-4 (c-erb-B-4). All members of the family have an extracellular ligand binding domain, a transmembrane domain, and a cytoplasmic tyrosine kinase domain, which for HER-3 is nonfunctioning [1–5]. HER-3 protein exists in normal human adult and fetal tissues, including the breast, and has also been shown to be expressed at both the mRNA and protein levels in a number of tumor cell lines and primary tumor material [6,7]. Normal HER-3 level in a healthy person ranges from 0.06 ng mL^{-1} to 2.55 ng mL^{-1}. Moreover, in a risk of cancer, the abnormal levels of HER-3 should be increased up to 12 ng mL^{-1}. [8].

HER-3 protein has been found to be over expressed in a range of tumors including those of the breast [9] and non-small-cell lung

* Corresponding author. Tel.: +90 282 250 2605; fax: +90 282 250 9925.
E-mail addresses: msezginturk@hotmail.com, msezginturk@nku.edu.tr (M.K. Sezgintürk).

0003-2670/$ – see front matter © 2014 Elsevier B.V. All rights reserved.
http://dx.doi.org/10.1016/j.aca.2014.01.041

carcinoma [10]. Since determination of c-erbB-3 in blood or tissues is essential, many methods such as immunohistochemical [11], enzyme linked immuno assay (ELISA) [12], and Western blot [13] have been reported to detect c-erbB-3.

Recently, electrochemical impedance spectroscopy (EIS) was used effectively for identification of membranes, biosensor characterization and fabrication with the help of cyclic voltammetry [14–17]. In fact, like electrical resistance, electrochemical impedance can be conceived as a measure of the ability of a circuit to resist the flow of electrical current, however unlike electrical resistance, electrochemical impedance is dependent of frequency and usually measured by applying an AC voltage to an electrochemical cell and then measuring the current through the cell [18–20]. However, in this study a novel impedance method has been applied to the immunosensor proposed based on gold nanoparticles. "Single frequency impedance" was performed to reveal binding the characteristics between HER-3 and anti-HER-3 attached to the biosensor surface. In electrochemistry, in order to discover surfaces of working electrodes, several methods such as scanning electrochemical microscopy, scanning tunneling microscopy, and scanning reference electrodes should be operated. However, using these methods to potential researchers is commonly time consuming and requires expensive equipments. Moreover scanning electron microscope (SEM) and atomic force microscope (AFM) should also be used for surface characterization of the biosensors. As is well known, both of these equipments are extremely expensive and in any laboratory SEM/AFM should not be provided. Consequently, as a valuable alternative way, measurements can be performed across the electrode at a single frequency to create an image of the electrode or, alternatively, performed at a given location to create a complete spectrum. In other words, single frequency impedance measurements can be performed to monitor the changes in the surfaces of the biosensors.

Self-assembly process is the spontaneous organization of substances into specific metal surfaces. Self assembled monolayer (SAM) of different substances have frequently utilized for development biosensors, microarrays, biochips, and molecular switches [21]. There are several advantages for the use of SAMs as a platform for immobilization of biomolecules such as easy formation of SAMs, providing suitable surface for biomolecule immobilization, flexibility to design the head group of SAM with various functional ends, and small amount of biomolecule is needed for immobilization on SAM [22].

In the current study, anti-HER-3 antibody was used as a biorecognition element for the first time to quantify HER-3. Self-assembly of hexanedithiol on a gold electrode was successfully performed and evaluated. Gold nanoparticles were used to enhance the surface area of a SAM modified electrode. Cysteamine monolayers were self-assembled on the gold nanoparticles. For immobilization of anti-HER-3, glutaraldehyde was used as a crosslinking agent. Immobilization steps were monitored by EIS and CV. For analyzing EIS data it fitted to an equivalent circuit model. Certain important parameters were optimized to obtain the best biosensor results. Finally, artificial serum samples spiked with HER-3 were analyzed by the biosensor.

2. Experimental

2.1. Materials and instrumentation

All reagents were purchased from Sigma–Aldrich (St. Louis, MO, USA) and were of analytical purity unless stated otherwise. HER-3 and anti-HER-3 were purchased from Sigma–Aldrich (St. Louis, MO, USA). For all dilutions, sterile phosphate buffers (pH 7, 0.01 M) were used. Anti-HER-3 and HER-3 portions were prepared at certain concentrations and were stored at −20 °C until use. Artificial serum solution was prepared using 4.5 mM KCl, 5 mM $CaCl_2$, 4.7 mM D(+)-glucose, 2.5 mM urea, 0.1% bovine serum albumin, and 145 mM NaCl. A three-electrode system, consisting of a gold working electrode (with a surface area of 2.01 mm^2), an Ag/AgCl (saturated KCl) reference electrode and a Pt counter electrode, was fabricated in a 10 mL electrochemical cell (all the electrodes were obtained from iBAS, Warwickshire, UK). Electrochemical experiments were performed using a Gamry Potentiostat/Galvanostat, Reference 600 (Gamry Instruments, Warminster, USA) interfaced with a PC via an EChem Analyst containing physical electrochemistry, pulse voltammetry, and electrochemical impedance spectroscopy software (Gamry Instruments, Warminster, USA).

2.2. Preparation of the self-assembled monolayer of hexanedithiol

Firstly, the surfaces of the Au electrodes were polished with 0.05 μm alumina and then washed ultrasonically in ethanol for 5 min to remove alumina particles. Then the electrodes were immersed in piranha (H_2O_2/H_2SO_4, 1/3 v/v) solution for 3 min. Afterwards, the electrodes were washed by immersion in ultrapure water ten times. For the next step, the surfaces of the electrodes were dried in a pure argon stream. This polishing and cleaning procedure was repeated before every electrode preparation step. The clean gold electrodes were immersed in a hexanedithiol solution (0.1 M, in pure ethanol) for 24 h. After this period, they were rinsed with ethanol and carefully dried with an argon gas.

2.3. Preparation of gold nanoparticles

2.4 mL of 40 mM sodium boron hydride ($NaBH_4$) was added to 50 mL 200 ppm $HAuCl_4$. Finally, gold electrodes were immersed in this solution for 24 h in a dark ambient. At the end of this step, the electrodes were flushed with ultra-pure water and dried with argon gas gently.

2.4. Covalent immobilization of anti-HER-3 on a modified gold electrode

Thereinafter, the electrodes were immediately immersed in a cysteamine solution (0.5 M in pure ethanol) and left overnight in the dark. After this period, they were rinsed with ethanol and gently dried in an argon stream. For the activation of amino ends, 5 μL 5% glutaraldehyde solution and 5 μL anti-HER-3 (5 μg μL^{-1}) were applied to the electrodes surfaces modified with cysteamine (Au/Cys) by a pipette. The electrodes were incubated for an hour in a moisture medium. Finally the electrodes were immersed in ultrapure water to remove physically adsorbed anti-HER-3 molecules. After washing the surfaces of the electrodes, 10 μL BSA solutions (1%) were dripped onto the electrode to block the active ends of the surfaces and this continued for an hour in a humid environment.

2.5. Electrochemical measurements

Cyclic voltammetry was used to characterize SAM formation on the bare gold electrodes, and the modified electrodes with different layers. The potential was varied between 0 and 500 mV (step size: 20 mV, scan rate: 50 mV s^{-1}) in the presence of a 5 mM $K_3[Fe(CN)_6]/K_4[Fe(CN)_6]$ (1:1) solution which served as a redox probe containing 0.1 M KCl. For electrochemical impedance studies, an alternating wave of 10 mV amplitude was applied to the electrode over the formal potential of the redox couple (0 V). The redox couple used for the impedance studies was the same as cyclic

voltammetry. Impedance spectra were collected in the frequency range between 10,000 and 0.05 Hz.

2.6. Measurement procedure

After each of the anti-HER-3 biosensors was immobilized, the biosensor surface was used to interact with the HER-3 solution. The standard solution of HER-3 was injected onto the biosensor surface by a micro-pipette. The concentrations of standard HER-3 solutions were 0.2 pg μL^{-1}. For each time measurement, the injection volume was 5 μL. The response value was measured after 1 h of incubation in a moisture medium. After the incubation period, the biosensor was gently immersed into the ultra-pure water ten times to remove physically adsorbed HER-3 molecules. Finally, the biosensor was again put into the cell containing the $Fe(CN)_6^{4-/3-}$ redox probe solution, and the electrochemical measurements were taken as described in the previous section. The difference in charge transfer resistance between the biosensor unbounded and bounded HER-3 was used for preparing the HER-3 calibration curves.

3. Results and discussion

In this study, CV and EIS were used to determine the changes on the surfaces of the gold electrodes during the anti-HER-3 immobilization processes. The redox couple of $Fe(CN)_6^{3-/4-}$ displayed good integrity of SAM on gold electrodes, for investigating the insulating properties, defect structure, and the density of the adsorbed layer [20,23]. Initially, it must be emphasized that the most important step for self-assembled monolayer formation is the cleaning of the gold electrode. A well-defined characteristic voltammogram of the redox couple could be observed on the bare gold electrode (Fig. 1A).

It was evident that the anodic and cathodic current at the gold electrode decreased after self-assembly of hexanedithiol on the gold electrode surface. Hexanedithiol acts as the initial driving force for the surface concentration, which leads to assembly due to the medium strength interaction of sulfur with gold. Next, there is the backbone component that is typically a chain of methylene carbons [24]. This was because hexanedithiol has a long carbon chain and made molecular packing structure so; a strong insulating layer was constituted. The hydrophobic effect was blocked by this layer and as a result, the transfer of electrons toward the electrode surface was hindered. Moreover, important advantages of using hexanedithiol SAM on a gold electrode can be noticed as gold is a relatively inert metal and resistive to any oxidation reaction and long-chain of hexanedithiol formed densely SAM due to van der Waals forces between its long carbon chain. Another advantage was the simple preparation of hexanedithiol SAM not requiring expensive equipment or extensive experience to be performed successfully. Anodic and cathodic currents related to the electrode surface after modification of the gold nanoparticles increased considerably. After the next step, cysteamine was bound to the gold nanoparticles by sulfur terminals. Moreover, amino terminals could also be bound by cysteamine. However, for this reaction, the pH should be 9.0. So in the experiments we used a phosphate buffer with pH 7.0. As can be seen from Fig. 1, the peak currents were more increased. However, after anti-HER-3 modification the cathodic and anodic currents were considerably decreased by the blocking effect of anti-HER-3. Bovine serum albumin, which was used to block active cysteamine ends, also decreased the peak currents through the same effect of anti-HER-3. These decreases in peak currents were attributed to the fact that anti-HER-3 and BSA isolated the surface and effectively prevented the transfer of electrons to the electrode surface.

Electrochemical impedance spectroscopy (EIS) is very effective technique for examining the material on the electrode surface. In a Nyquist plot, the semicircle diameter at higher frequencies corresponds to the electron-transfer resistance (R_{ct}) and the linear part at lower frequencies corresponds to the diffusion process (Warburg impedance). Furthermore, the larger the semicircle diameter in the complex plane, the larger the value of R_{ct}. The diameter of the semicircle also showed the blocking behavior of the modified electrode after each modification step. In the presented experiments, R_{ct} values were calculated by means of an equivalent circuit model inserted in Fig. 1B. Here, R_s = resistance of the working solution, CPE (constant phase element) = connected with the capacitance of the complex bioactive layer. R_{et} shows electron transfer resistance through the electrode surface, and the Warburg impedance, Z_w, describes the normal diffusion to the electrode surface through the complex layer. The self-assembly of hexanedithiol onto gold electrode resulted in a dramatically increase in charge transfer resistance (Fig. 1B). Because SAM of hexanedithiol formed an effective insulating layer against to the diffusion of redox probe. On the contrary, after modification of the gold nanoparticles, electron transfer resistance considerably decreased. This reduction was caused by the good conducting properties of the gold nanoparticles. The excellent biocompatibility, conductivity and catalytic properties of gold nanoparticles have frequently been reported in many biosensor studies. When the surface of gold electrode was covered by considerable insulating hexanedithiol monolayer, the electron transfer between the bulk solution and the electrode surface was blocked resulting into increase in charge transfer resistance. However, after modification of gold nanoparticles, because the excellent conductivity of gold nanoparticles enhanced the electron transfer between the bulk solution and the electrode surface and probably they acted as electron transfer wires.

Moreover, electrochemical impedance studies showed that the electron transfer resistance was decreased more by modification of cysteamine (Fig. 1B). Amino groups attract the negative charges of the redox probe so the electron transfer resistance decreases. This result also clearly suggested that the cationic, protonated amino group of cysteamine attracted $Fe(CN)_6^{3-}$ electrostatically and/or induced a partial adsorption of $Fe(CN)_6^{3-}$ onto the electrode surface. The decreases in peak currents resulted from binding of anti-HER-3, and BSA also appeared as certain increases in charge transfer resistances as expected. This was due to the insulating properties of anti-HER-3 and BSA.

3.1. Optimization steps

The construction steps of the anti-HER-3-based biosensor were investigated especially in regard to incubation periods and concentration of hexanedithiol, cysteamine and anti-HER-3 concentrations. Details are given below.

First of all, to evaluate the effect of the period of hexanedithiol SAM formation on the biosensor construction, different incubation periods such as six hours and overnight were used. The results showed that an increase in the time period effectively increased the charge transfer resistance. Consequently, the overnight time period was chosen for the best results. In fact the results showed that a layer forms on a gold surface over one hour. Even at the end of the six hours, considerable charge transfer resistance was observed. However, on this electrode it was not possible to immobilize anti-HER-3 effectively. It is likely that a disordered monolayer was assembled in a few minutes, and the thickness of the layer reached very close to its maximum value. After this initial step, the most important process related to van der Waals forces should supposedly be started. The van der Waals forces between the hydrocarbon chains of hexanedithiol pack the molecules into a well-ordered structure. By this process hydrocarbon chains are well-ordered and ordering defects should be removed.

Also, different concentrations of hexanedithiol were used namely 10 mM and 100 mM. 10 mM did not significantly affect

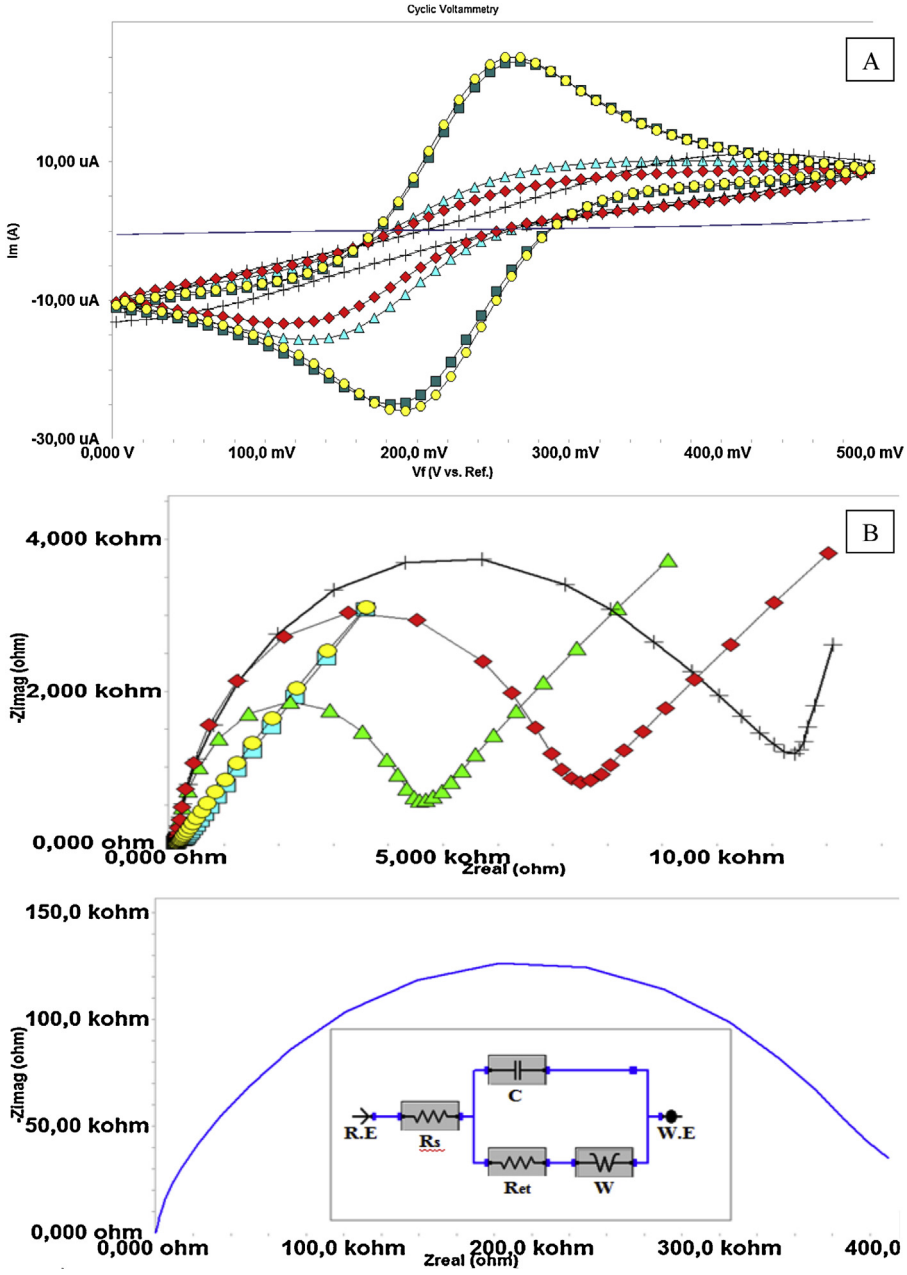

Fig. 1. Electrochemical characterization of gold nanoparticle based biosensor >[(A) cyclic voltammograms of anti-HER-3 immobilization steps >(B) electrochemical impedance spectra of HER-3 immobilization steps [(■-) bare Au, blue straight line: Au/HDT, (+): Au/HDT/AuNP, (●): Au/HDT/AuNP/Cys, (▲): Au/HDT/AuNP/Cys/anti-HER-3, (♦): Au/HDT/AuNP/Cys/anti-HER-3/BSA]. (For interpretation of the references to color in this figure legend, the reader is referred to the web version of this article.)

the response, and an increase in the hexanedithiol concentration resulted in an increase in the charge transfer resistance. Therefore, the 100 mM concentration was chosen. The concentration of hexanedithiol was an important parameter. Poirier and Pylant [25] reported that at low surface coverage, the alkanethiolate molecules lie flat with their hydrocarbon backbones parallel to the gold surface; at higher surface coverages, the molecules begin to stand up, with the hydrocarbon tails tilting approximately 30° from the surface in the all-trans configuration so as to maximize the van der Waals interactions. The results presented here were in absolute agreement with this previously reported theory.

The next step in the optimization studies was the determination of optimum cysteamine concentration. The experiments showed that the response of a biosensor would be affected by the concentration of cysteamine. Hence, different concentrations such as 0.01, 0.05, 0.1, 0.25 and 0.5 M were examined. The results are given in Fig. 2.

Increasing the concentration of cysteamine resulted in a decrease in the charge transfer resistance. Also R_{ct} values were calculated to find the optimum cysteamine concentration. The experiments revealed that cysteamine concentration influenced the biosensor response. A decrease in cysteamine concentration brought about a decrease in biosensor signal levels. This was an expected result because insufficient formation of SAM by cysteamine probably occurred. Consequently anti-HER-3 immobilization was not effectively achieved with low cysteamine concentrations. Moreover when discussing the affinity of cysteamine for gold, because of the shorter alkane chain of cysteamine it possibly assembled hardly compared to hexanedithiol. The strong

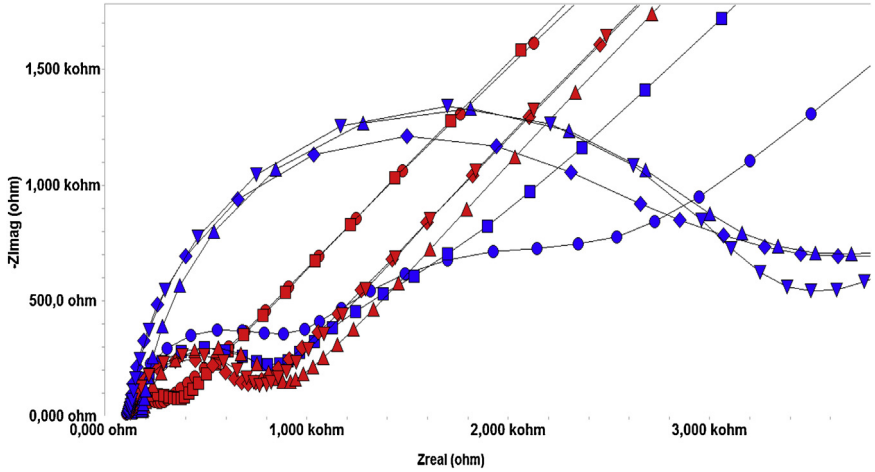

Fig. 2. The effect of cysteamin concentration on biosensor signals [The red traces show impedance spectra obtained before HER-3 application (Au/HDT/AuNP/Cys/anti-HER-3/BSA). The blue traces show impedance spectra obtained after 1.4 pg mL^{-1} HER-3 applications. Cysteamin concentrations performed: (●): 0.01 M, (■-): 0.05 M, (▲): 0.1 M, (♦): 0.25 M, (▼): 0.5 M]. (For interpretation of the references to color in this figure legend, the reader is referred to the web version of this article.)

SAM formation of cysteamine resulted in the effective binding of anti-HER-3. Consequently an increase in the concentration of cysteamine also increased the performance of anti-HER-3 immobilization. R_{ct} values, obtained for 1.4 pg mL^{-1} of HER-3, 1768, 809, 3223, 3425, and 3255 Ω, were calculated for different cysteamine concentrations such as 0.01 M, 0.05 M, 0.1 M, 0.25 M and 0.5 M respectively. When the cysteamine concentrations were higher than 0.1 M, the results were almost the same. However, the charge transfer resistance differences among HER-3 injections were more obvious than the others if 0.5 M cysteamine was used. As a result, for the best results, 0.5 M cysteamine was chosen.

Another parameter was the best concentration of glutaraldehyde, and several concentrations were examined including 1%, 1.5%, 2.5%, 3.5%, 5%, 7.5% and 10%. Glutaraldehyde is a reactive crosslinking agent that binds amine groups located on cysteamine. The results showed that when the concentration of glutaraldehyde increased, the achievement of anti-HER-3 immobilization considerably increased. On the other hand, high crosslinking degrees were revealed to be effective in lowering the activity of anti-HER-3 towards HER-3 because of possible denaturation. Consequently, 5% of glutaraldehyde was chosen as the optimum concentration.

Finally, different concentrations of anti-HER-3 were tried in an attempt to obtain the optimum concentration of anti-HER-3. For this purpose, different concentrations of anti-HER-3 portions (1 μg μL^{-1}, 2 μg μL^{-1}, 5 μg μL^{-1}, 10 μg μL^{-1} and 20 μg μL^{-1}) were tested. R_{ct} values for each concentration were calculated as 284, 1628, 2503, 2278 and 1048 Ω, respectively. The blocking behavior of anti-HER-3 on the electrode surface for the redox probe $Fe(CN)_6^{3-/4}$, caused an increase in the charge transfer resistance. When we used anti-HER-3 concentrations higher than 10 μg μL^{-1}, probably the higher crosslinking ratio because of the using higher anti-HER-3 amounts, they yielded anti-HER-3 proteins immobilized at very high densities. Consequently immobilization of anti-HER-3 molecules with high density negatively affected the biosensor response. As shown in the figure, the biosensors utilizing 10 μg μL^{-1} and 5 μg μL^{-1} showed similar results. As a consequence, 5 μg μL^{-1} of anti-HER-3 portion was used for further studies.

3.2. Analytical characteristics of the anti-HER-3 biosensor

In this study, under optimal conditions HER-3 was detected by the developed biosensor. As shown in the Fig. 3A, the peak values decreased with an increase in HER-3 concentration applied to the biosensor. Moreover, as can be seen in Fig. 3B, when the HER-3 concentration increased, the charge transfer resistance increased also. The reason for this increment was that an insulating layer was formed on the electrode surface. The diffusion of the redox probe $[Fe(CN)_6]^{3-/4-}$ was limited because of the insulating effect of HER-3. Moreover, the semicircle radius increased after HER-3 addition to the biosensor surface.

A calibration graph for HER-3 was drawn that shows the differences in charge transfer resistances after HER-3 binding. The calibration graph is given in Fig. 4.

The change in charge transfer resistance differences (ΔR_{ct}) was calculated by the following equation:

$$\Delta R_{ct} = R_{ct(\text{Anti-HER-3/BSA/HER-3})} - R_{ct(\text{Anti-HER-3/BSA})}$$

The reproducibility of the new anti-HER-3-based biosensor was also assessed. The reproducibility of eleven exact biosensors was examined. In addition, the calibration curves were obtained from the impedimetric responses of the nine biosensors. The results are given in Table 1.

The charge transfer resistances of the biosensor were investigated when the biosensor was consecutively exposed to a 0.2 pg mL^{-1} HER-3 standard solution seven times. The repeatability of the measurements was very good considering that the correlation coefficient on measurements was 6.19%, and the average value and standard deviation were calculated as 0.21 pg mL^{-1} and ±0.013 pg mL^{-1}, respectively. The results showed that the biosensor exhibited the desirable analytical feature of repeatability.

As previously mentioned the biosensor presented in the manuscript is the first immunosensor system for analysis of HER-3 in the literature. The methods developed for the determination of HER-3 are based on the immunohistochemical or ELISA (enzyme-linked immunosorbent assay) procedures. For instance, a commercially available HER-3 ELISA kit employs an antibody specific for human HER-3 coated on a plate. The analysis procedure of this technique contains time consuming steps. Moreover, the cost of an assay kit is extremely expensive (400 Euros). However, the cost of one ITO based immunosensor developed is approximately 0.01 Euros. The minimum detectable level of HER-3 is reported as typically less than 4 pg mL^{-1}. This limit is similar to the immunosensor presented here.

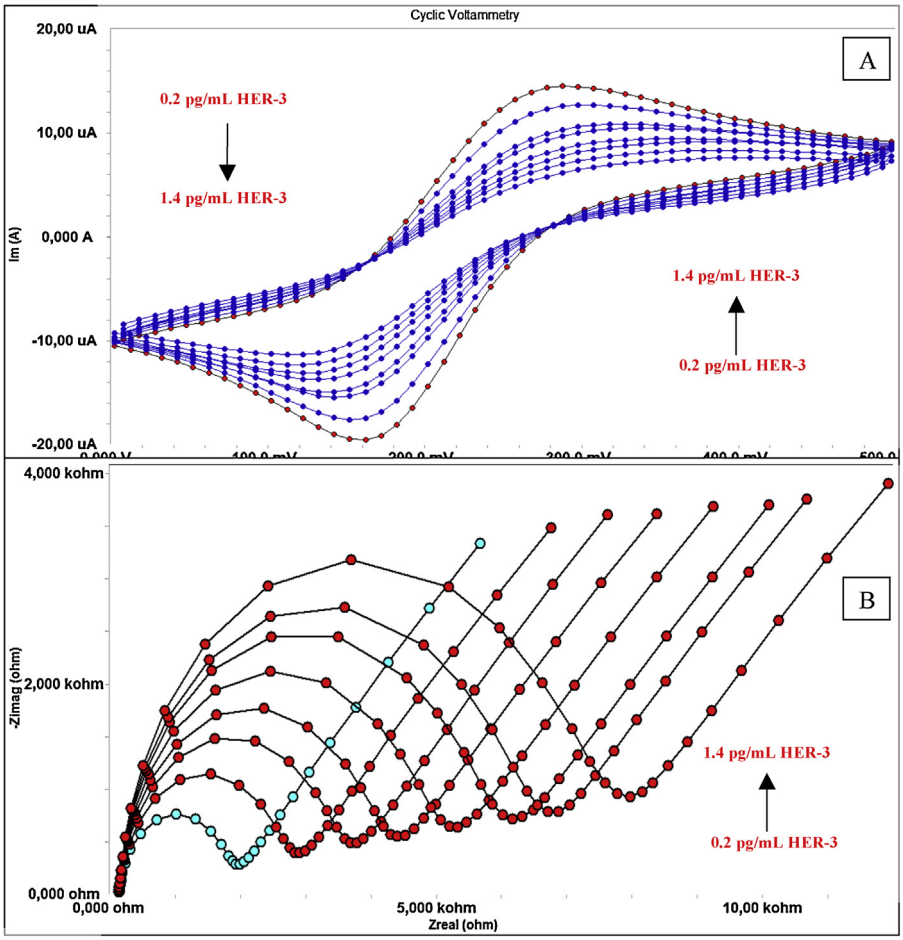

Fig. 3. Cyclic voltammograms (A) and impedance spectrums (B) obtained for different concentrations of HER-3 by the presented anti-HER-3 biosensor.

Table 1
Kramers–Kronig transforms for different layers of the biosensor.

Biosensor surfaces	Goodness of fit values
Bare Au	6.302
Au/HDT	17.92
Au/HDT/AuNP	5.1
Au/HDT/AuNP/Cys	6.586
Au/HDT/AuNP/Cys/anti-HER-3	11.80
Au/HDT/AuNP/Cys/anti-HER-3/BSA	16.67
Au/HDT/AuNP/Cys/anti-HER-3/BSA/HER-3	2.376

Reproducibility of the biosensor

Biosensor numbers	R^2	y	Linear ranges (pg mL^{-1})
1	0.9804	$733.21x - 65.929$	0.2–1.4
2	0.9951	$4714.1x - 40.714$	0.2–1.4
3	0.9952	$928.52x + 38.5$	0.2–1.4
4	0.9939	$2726.1x + 40.214$	0.2–1.4
5	0.9888	$4826.8x + 30$	0.2–1.4
6	0.9981	$3988.8x + 22.286$	0.2–1.4
7	0.9887	$350.99x - 117.94$	0.2–1.4
8	0.9802	$2117.5x - 265.81$	0.2–1.4
9	0.9874	$212.21x - 48.4$	0.2–1.4

HER-3 detection in artificial serum samples

HER-3 (pg mL^{-1})				
Added	Found by the biosensor	% Recovery	% Relative differences	Standard deviations (pg mL^{-1})[a]
0.2	0.214	107	7	±0.060
0.6	0.633	105.5	5.5	±0.031
1.0	1.04	104	4	±0.056

[a] Standard deviations were calculated from four measurements.

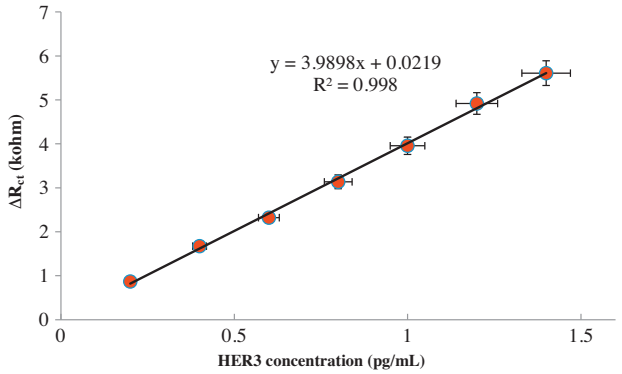

Fig. 4. HER-3 calibration curve obtained by gold nanoparticle based biosensor for anti-HER-3.

The Kramers–Kronig relations are integral equations in which real and imaginary components of complex quantities for systems are restrained. Moreover, these complex quantities satisfy the conditions of linearity, causality, and stability [26–28]. In principle, the Kramers–Kronig relations can be used to determine whether the impedance spectrum of a given system has been influenced by bias errors caused, for example, by instrumental artifacts or time-dependent phenomena [28]. In this present work, the software called Gamry Echem Analyst (Ver. 5.61) was used to perform Kramers–Kronig transforms. The calculation was carried out following the method used by Boukamp [29]. To calculate the real part of a linear, stable, and causal circuit, imaginary part of the experimental data was used. According to these calculations, a value named "goodness of fit" was procured. For the present new biosensor, Kramers–Kronig Transforms were performed for all steps including preparation of the biosensor and measurement. The goodness of fit values of different biosensor surfaces are also given in Table 1. The Kramers–Kronig Transforms performed on the electrochemical impedance spectra related to the biosensor revealed that the experimental data agreed with the data obtained by the transform. The impedance spectra obtained by means of the Kramers–Kronig Transforms were fitted to data obtained by experiments and all overlaying spectra are shown in Fig. 5.

Nevertheless, it was very important that the impedance spectra were linear, stable, and causal circuits. Finally, it was also significant that the system was not influenced by unknown variables.

Moreover, in this study a new impedimetric technique was applied to the biosensor for the first time. In the literature, electrochemical impedance spectroscopy is used for the immobilization and characterization of a biosensor. It is also utilized to analyze the charge transfer resistances of a modified surface. In order to characterize the binding of HER-3 to anti-HER-3, which was immobilized onto the electrode surface, the "single frequency impedance" technique was performed successfully. Single frequency impedance measures the impedance at a fixed frequency versus time. Consequently it should be possible to control the experiment with a repeat time and a total time. For this purpose, the potentiostat was set up at a fixed frequency of 500 Hz. The HER-3-related variation of impedance was observed in the relatively low-frequency range (0.1–1 kHz) and the Bode plot analysis of HER-3 determination corroborated this finding. The Bode plots represent frequency information. In a Bode plot, the impedance is plotted with log frequency on the *x*-axis and both the absolute values of the impedance and the phase-shift on the *y*-axis. Consequently, the highest change in phase-shift related with HER-3 binding should be associated with HER-3 concentration and should provide information on frequency. The rate of impedance change was much higher for relatively low frequency signals (0.1–1 kHz) than for the greater frequency regions (higher than 1 kHz). Eventually, single frequency measurements were conducted at a fixed frequency, 500 Hz. The impedance was measured at this fixed frequency as a function of time and phase angle for 60 min. The result is shown in Fig. 6.

When HER-3 was applied onto the biosensor surface, the impedance magnitude started to increase as shown in Fig. 6 and the magnitude of impedance reached steady state approximately after 50 min. This result also corroborated the measurement procedure of the biosensor mentioned in the Section 2.6. Since, we used an hour incubation period for the interaction between anti-HER-3 and HER-3 in all experiments. Eventually, single frequency impedance should be performed to evaluate biosensor signals, process monitoring, or to evaluate slow time-dependent changes in a biosensor surface. The results also revealed that single frequency experiments could give very important information on binding kinetics of an antibody and antigen. The results also revealed that this method should be used as a reliable approach for real time monitoring of analytes.

Finally the proposed anti-HER-3 based biosensor was employed to determine HER-3 content in artificial serum samples. The results are shown in Table 1. The data were in good agreement between the added amount and the detected amount.

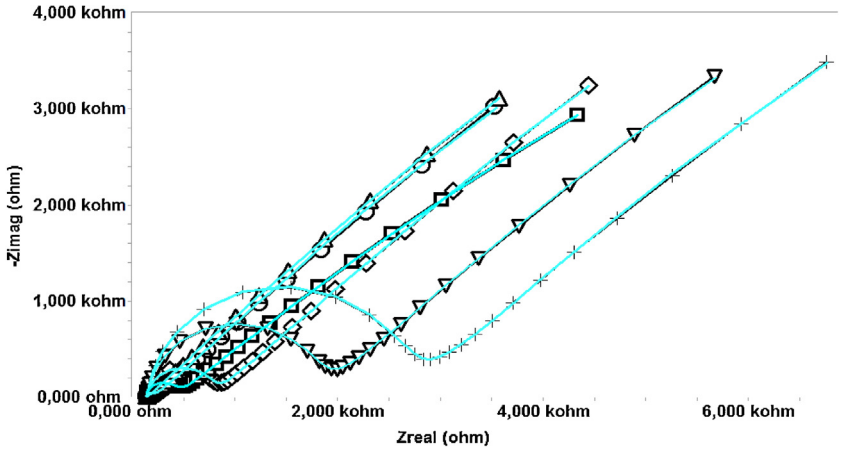

Fig. 5. The plots of Kramers–Kronig transforms performed on different layers of the presented biosensor. [The turquoise blue lines show Kramers–Kronig transforms performed and fitted on the experimental data and the black lines show experimental results. (●): bare Au, (■): Au/HDT/AuNP, (▲): Au/HDT/AuNP/Cys, (♦): Au/HDT/AuNP/Cys/anti-HER-3, (▼): Au/HDT/AuNP/Cys/anti-HER-3/BSA, (+): Au/HDT/AuNP/Cys/anti-HER-3/BSA/HER-3]. (For interpretation of the references to color in this figure legend, the reader is referred to the web version of this article.)

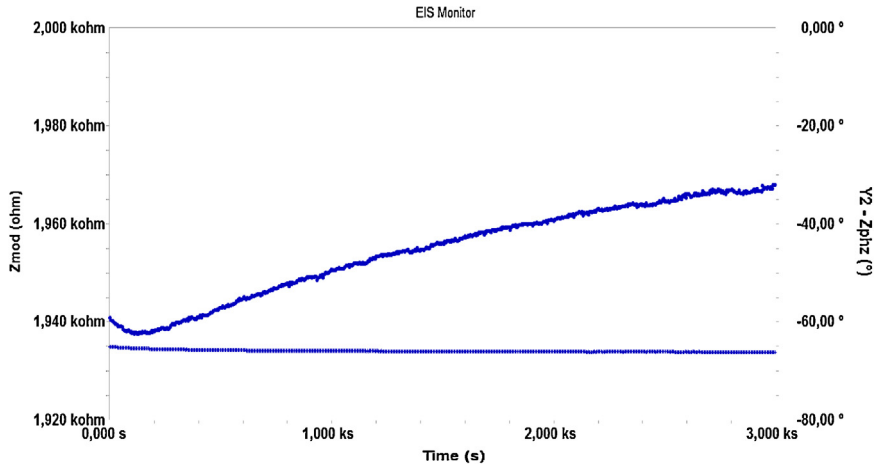

Fig. 6. Single frequency impedance measurement.

4. Conclusion

In conclusion, a novel anti-HER-3 immunosensor was constructed to develop a biosensor for early detection of HER-3. Anti-HER-3 antibody was used as a biorecognition element for the first time by the proposed biosensor system. The SAM of the hexanedithiol surface area was used as an immobilization layer. Gold nanoparticles and cysteamine were utilized to improve the sensitivity of detection. The proposed anti-HER-3 biosensor demonstrated high sensitivity, a wide linear range, good reproducibility, and acceptable precision and accuracy. The Kramers–Kronig transforms revealed that the whole biosensor system was linear, stable, and formed a causal circuit. Moreover, single frequency impedance analyses were carried out to identify the binding characteristics of HER-3 and anti-HER-3 for the first time in such a biosensor system. Based on our results, it is highly recommended that the single frequency impedance can be employed for different biosensor applications such as for evaluation or to clarify slow time-dependent changes on a biosensor surface. This electrochemical technique should make continuous and rapid measurements possible with a very low cost potentiostat. Finally, this biosensor was successfully applied to HER-3 analysis of artificial serum samples.

Acknowledgment

This work was supported by a grant from TÜBİTAK (The Scientific and Technological Research Council of Turkey, Project number: 109T 172).

References

[1] C.L. Arteaga, Semin. Oncol. 29 (2002) 3–9.
[2] A. Berchuck, G. Rodriguez, A. Kamel, Obstet. Gynecol. 76 (1990) 381–387.
[3] S.M. Tovey, C.J. Witton, J.M. Bartlett, Breast Cancer Res. 6 (2004) 246–251.
[4] C.J. Witton, J.R. Reeves, J.J. Going, J. Pathol. 200 (2003) 290–297.
[5] J. Woodburn, D.E. Turner, P.S. Helliwell, S. Barker, Rheumatology 38 (12) (1999) 1260–1268.
[6] N.R. Lemoine, D.M. Barnes, D.P. Hollywood, C.M. Hughes, P. Smith, E. Dublin, S.A. Prigent, W.J. Gullick, H.C. Hurst, Br. J. Cancer 66 (6) (1992) 1116–1121.
[7] T. Rajkumar, W.J. Gullick, Br. J. Cancer 70 (1994) 459–465.
[8] S.H. Lin, Y.C. Lee, M.B. Choueiri, S. Wen, P. Mathew, X. Ye, K.A. Do, N.M. Navone, J. Kim, S.M. Tu, L.Y. Yu-Lee, C.J. Logothetis, Clin. Cancer Res. 14 (12) (2008) 3729–3736.
[9] A.K. Koutras, K.T. Kalogeras, M.A. Dimopoulos, R.M. Wirtz, U. Dafni, E. Briasoulis, D. Pectasides, H. Gogas, C. Christodoulou, G. Aravantinos, G. Zografos, E. Timotheadou, P. Papakostas, H. Linardou, E. Razis, T. Economopoulos, H.P. Kalofonos, G. Fountzilas, Br. J. Cancer 99 (2008) 1775–1785.
[10] L.R. Hirsch, R.J. Stafford, J.A. Bankson, S.R. Sershen, B. Rivera, R.E. Price, J.D. Hazle, N.J. Halas, J.L. West, Proc. Natl. Acad. Sci. USA 100 (2003) 13549–13554.
[11] W. Hilbe, S. Dirnhofer, F. Oberwasserlechner, W. Eisterer, K. Ammann, T. Schmid, J. Clin. Pathol. 56 (2003) 736–741.
[12] A.C. Hsieh, M.M. Moasser, Br. J. Cancer 97 (2007) 453–457.
[13] L. Göstring, M. Malm, I. Höidén-Guthenberg, F.Y. Frejd, S. Ståhl, J. Löfblom, G. Gedda, PloS One 7 (6) (2012) 1371–1376.
[14] J. Ezzati, N. Dolatabadi, O. Mashinchian, B. Ayoubi, A.A. Jamali, A. Mobed, D. Losic, Y. Omidi, M. Guardia, Trends Anal. Chem. 30 (2011) 459–472.
[15] R.B. Queirós, N. Santos-Álvarez, J.P. Noronha, M.G.F. Sales, Sens. Actuat. B: Chem. 181 (2013) 766–772.
[16] W. Chen, Y.H. Liu, H. Li, A. Liu, X. Lin, Y. Chen, Anal. Chim. Acta 748 (2012) 89–94.
[17] R. Ohno, H. Ohnuki, H. Wang, T. Yokoyama, H. Endo, D. Tsuya, M. Izumi, Biosens. Bioelectron. 40 (2013) 422–4266.
[18] E. Barsoukov, J.R. Macdonald, Impedance Spectroscopy: Theory, Experiment, and Applications, 2nd, Wiley Interscience Publications, 2005.
[19] A.J. Bard, L.R. Faulkner, Electrochemical Methods: Fundamentals and Applications, Wiley Interscience Publications, 2000.
[20] L. Qingwen, G. Hong, W. Yiming, L. Guoan, M. Jie, Electroanalysis 13 (2001) 1342–1346.
[21] C. Engtrakul, L.R. Sita, Nano Lett. 1 (2001) 541–549.
[22] N.K. Chaki, K. Vijayamohanan, Biosens. Bioelectron. 17 (2002) 1–12.
[23] R. Pei, Z. Cheng, E. Wang, X. Yang, Biosens. Bioelectron. 16 (2001) 355–361.
[24] L. Strong, G.M. Whitesides, Langmuir 4 (1988) 546–558.
[25] G.E. Poirier, E.D. Pylant, Science 272 (1996) 1145.
[26] R.de.L. Kronig, J. Opt. Soc. Am./Rev. Sci. Instrum. 12 (1926) 547–557.
[27] H.A. Kramers, Physik. Z. 30 (1929) 522–523.
[28] M.E. Orazem, B. Tribollet, Electrochemical Impedance Spectroscopy, Wiley, New Jersey, 2008.
[29] B.A. Boukamp, J. Electrochem. Soc. 142 (1995) 1885–1894.